Lab on a Chip

Accepted Manuscript

ROYAL SOCIETY OF CHEMISTRY

www.rsc.org/loc

Continuous-Flow Sorting of Stem Cells and Differentiation Products based on Dielectrophoresis

Hongjun Song[a], Jenna M. Rosano[a], Yi Wang[*a], Charles J. Garson[a], Balabhaskar Prabhakarpandian [a], Kapil Pant[a]
[a] CFD Research Corporation, 701 McMillian Way NW, Huntsville, AL, 35806, U.S.A.

George J. Klarmann[b], Alan Perantoni[b], Luis M. Alvarez[b,c]
[b] Cancer and Developmental Biology Laboratory, National Cancer Institute, Frederick, MD 21702, U.S.A
[c] Department of Chemistry and Life Sciences, United States Military Academy, West Point, NY 10996 U.S.A.

Eva Lai[d,e]
[d] Department of Chemical and Biomolecular Engineering, Johns Hopkins University, 3400 N. Charles Street, Baltimore, MD 21218, U.S.A
[e] Telemedicine and Advanced Technology Research Center (TATRC), U.S. Army Medical Research and Materiel Command (USAMRMC), 1054 Patchel Street, Fort Detrick, MD 21702, U.S.A.

ABSTRACT:

This paper presents a continuous-flow microfluidic device for sorting stem cells and their differentiation progeny. The principle of the device is based on the accumulation of multiple dielectrophoresis (DEP) force to deflect cells laterally in conjunction with the alternating on/off electric field to manipulate the cell trajectories. The microfluidic device containing a large array of oblique interdigitated electrodes was fabricated using a combination of standard and soft lithography techniques to generate a PDMS-gold electrode construct. Experimental testing with human mesenchymal stem cells (hMSC) and their differentiation progeny (osteoblasts) was carried out at different flow rates, and clear separation of the two populations was achieved. Most of osteoblasts experiencing stronger DEP forces were deflected laterally and continuously, following zig-zig trajectories, and moved towards the desired collection outlet, whereas most of hMSCs remained on the original trajectory due to weaker DEP force. The experimental measurements were characterized and evaluated quantitatively, and consistent performance was demonstrated. Collection efficiency up to 92% and 67% for hMSCs and osteoblasts, respectively, along with purity up to 84% and 87% was obtained. The experimental results established the feasibility of our microfluidic DEP sorting device for continuous, label-free sorting of stem cells and their differentiation progenies.

Keywords: stem cell, differentiation, separation, microfluidic, continuous flow, dielectrophoresis

[*]Corresponding author
E-mail: yxw@cfdrc.com
Phone: +01-256-726-4915
Fax: +01-256-726-4806

1 Introduction

Stem cells offer a renewable source to repair and replace cells and tissues for the treatment of human injury and disease (i.e., regenerative medicine) [1-3]. Separation of stem cells and their differentiated derivatives plays a very important role in stem cell-based therapies and research [4]. Traditional methods for stem cell identification and sorting, such as flow cytometry [5] and fluorescence activated cell sorting (FACS) [6], require the use of fluorescent biomarkers, antibodies, or nanoparticles, which may alter the cellular properties, including limiting their applicability for therapies (e.g. by altering the cellular interactions, uptakes and/or engraftments) [7]. In addition, relevant and unique surface biomarkers may occur in low prevalence or may not be present at all in certain types of stem cells [7]. While impedance-based cell analysis can effectively monitor and identify stem cell differentiation status in a label-free and non-invasive manner [8-13], cell sorting techniques are typically entailed to isolate the differentiation progenies from the stem cells for regenerative therapeutics.

Dielectrophoresis (DEP) offers an attractive, non-invasive method to separate cells in heterogeneous populations based on their unique dielectric properties. DEP force is exerted on a cell when the suspended cell becomes polarized under a non-uniform electric field in a media with different dielectric properties [14]. DEP-based manipulation, such as trapping or continuous sorting has been successfully exploited to distinguish bacteria, mammalian cells, blood cells, cancer cells, human leukocytes, neural cell, circulating tumor cells, etc. [15-31]. Recently, the technique has also found broad applications in stem cell research [32], such as stem cell extraction and enrichment, as well as isolation of differentiated progeny [33-39]. DEP has been used to enrich hematopoietic stem cells from a mixed cell population in bone marrow [37, 38], as well as putative stem cells from enzyme-digested adipose tissue [39]. A DEP field-flow fractionation (DEP-FFF) device, fabricated on a novel flex-circuit, was employed to separate and enrich erythrocytes up to 14-fold [29]. Flanagan et al. [33] demonstrated how unique dielectric properties arising due to subtle phenotypic differences within a population of mouse neural stem/precursor cells (NPSCs) can be used to distinguish differentiation progeny. Based on their study, NSPCs may be isolated into populations that are either more likely to generate neurons or astrocytes via DEP. Similar DEP methods have also used to analyze the electrophysiological properties of cortical human and mouse NSPCs, demonstrating that the membrane capacitance of the cell inversely correlates to the neurogenic potential of NSPCs [34]. An automated DEP assisted cell sorting (DACS) device was developed for characterization and isolation of neural cells from a heterogeneous population of mouse derived NSPCs and neurons [36], in which a novel microfluidic DEP-based manifold was employed to enable sorting at discrete frequency bands rather than a single frequency. The inherent electrophysiological properties of whole cell membrane capacitance were used to define and separate two distinct population of NSPCs: one with more neurogenic progenitors and the other one with more astrogenic progenitors [35]. The study also correlated cell surface glycosylation (contributing to plasma membrane biophysical properties) to the cell fate electrophysiological properties, which can be used to isolate cells of differing fate potential in the neural lineage.

Most of the above approaches for stem cell separation and enrichment were based on batch-mode operation (i.e., trapping and release), and require precise sequential control of the applied electric field and valves to complete the process. In this paper, we describe the fabrication and application of a microfluidic DEP sorter to continuously separate human mesenchymal stem cells (hMSCs) and their differentiation progenies (osteoblasts). The innovation of the present effort lies in the combination of accumulation of multiple DEP-induced deflections along the lateral direction (realized by an array of oblique interdigitated electrodes) and AC electric field with alternating on/off control. It not only enables continuous operation, but also high cell recovery and collection efficiency, and is one of the most important elements distinguishing the present work from prior seminal research [33-39]. Further, this capability to facilitate rapid and accurate flow-based sorting in a closed system with disposable fluids could easily be sterilized and be made to be compatible with Good Manufacturing Practices

(GMP), which is a critical need to enable development and administration of safe and effective cell-based therapies for clinical use.

2 Principle and Design

In this section, we describe the principle and design of our microfluidic DEP-based sorting device for continuously separating stem cells from their differentiated products. The device consists of a microfluidic channel with a cell sample inlet, a buffer solution inlet, and two outlets (see Figure 1). An oblique interdigitated electrode array is located on the floor of the microfluidic channel, spanning the entire channel with an inclined angle of 45° relative to the flow direction. Samples containing a mixture of stem cells and their differentiated products are loaded into the cell sample inlet (top right in Figure 1), and a buffer solution is injected into the buffer solution inlet to serve as a sheath flow.

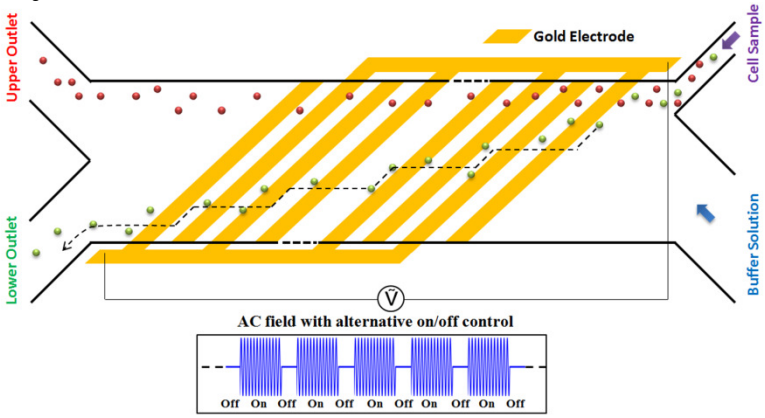

Figure 1. Schematic of principle and design for the continuous flow DEP-based microfluidic cell separation. The device consists of a microchannel connected to two inlets (cell sample and buffer solution) and two outlets. An array of oblique interdigitated electrodes inclined at 45° relative to the flow direction is located on the floor of the microchannel. An AC field with alternating on/off control is applied between the interdigitated electrodes for DEP generation.

Recent research has clearly confirmed that there are salient changes in morphology and membrane structure of the stem cells during differentiation [33-36], in particular, the membrane capacitance. This gives rise to the differential DEP forces acting on the stem cells and the differentiation products when they are polarized under non-uniform AC electric field. In our design, the electric field is generated between the interdigitated electrodes, and DEP force perpendicular to the electrode edge is exerted on the cells flowing over the electrodes in the microchannel. The time-averaged DEP force on a single cell (assumed spherical) may be expressed as [40]

$$F_{DEP} = 2\pi\varepsilon_m R^3 \,\mathrm{Re}(\beta)\nabla E^2 \quad \text{and} \quad \beta = (\varepsilon^*_{cell} - \varepsilon^*_m)/(\varepsilon^*_{cell} + 2\varepsilon^*_m) \tag{1}$$

where ε_m is permittivity of the medium, R is the radius of the cell, E is the strength of the applied electric field, β is the Clausius-Mossotti (CM) factor, and ∇ is the gradient operator. $\varepsilon^* = \varepsilon - i\sigma/\omega$ is the effective complex permittivity; ε and σ are the dielectric permittivity and electric conductivity, respectively, ω is the angular frequency of the applied electric field. Subscript "*cell*" and "*m*" denote the quantities for cell and medium, respectively. In case of Re(β) < 0 or Re(β) > 0, cells will be excluded from or attracted to the electrodes, which are termed positive or negative DEP, respectively. Eq. (1) also states that DEP force on cells can be tuned by virtue of frequency of the AC field or the buffer conductivity.

The key to clear separation is to identify an operating regime, in which Re(β) and DEP force on the two cell populations are different. As shown in Figure 1a, cells with larger Re(β) (colored in green) experience stronger DEP force, resulting in a larger lateral deflection than those with a smaller Re(β) (colored in red). Thus, the former can be collected at the lower outlet and the others at the upper outlet. Two points need to be noted regarding the operation of our device: First, DEP spectrum measurement

was performed to observe the DEP response behavior (e.g. positive and negative DEP) under various AC frequencies. Based on our observation, it was found that the optimal frequency generating the salient difference in Re(β) between hMSCs and their differentiated progeny (i.e., osteoblasts in this study) falls into the positive DEP regime, where many cells can be slowed down or even trapped at the electrode edges, leading to low cell recovery. To overcome this issue, an alternating on-off AC field rather than a continuous one is utilized as shown in Figure 1. The profile of the AC field is obtained by time-multiplexing a sine wave with a square wave. Second, in contrast to most continuous-flow DEP devices (e.g., focuser and sorter [20, 23, 24, 41]) that rely on negative DEP to exclude cells from the electrodes, the electrode array in our design is oblique and can operate in positive DEP mode, allow the cells to approach and pass over the electrodes, and accumulate the lateral movement. Cells are deflected and move laterally along the electrode due to DEP when the AC field is on, and migrate downstream along the flow direction when the AC field is off (without DEP). As a result, they form zigzag trajectories (dash line in Figure 1a) and finally are collected at the outlets.

3 Materials and Methods

3.1 Sample Preparation

Immortalized human mesenchymal stem cells (hMSCs) [42, 43] were cultured in low-glucose DMEM, supplemented with L-glutamine, sodium pyruvate, MEM (minimum essential medium) non-essential amino acid, and 10% MSC-qualified FBS (fetal bovine serum) (Life Technologies, Carlsbad, CA). When hMSCs were 80% confluent, the cells were treated with osteoblast induction media, composed of the aforementioned growth media accompanied by 50 μM ascorbic acid, 100 μM glycerol-2-phosphate, and 100 nM dexamethasone [44]. Induction media was changed every 2 to 3 days, and hMSCs fully differentiated into osteoblasts over a period of 21 days. Differentiation progression was monitored by observing cell morphology, alkaline phosphatase activity [45], and mineralization over 21 days. Cells were fixed and stained with either an alkaline phosphatase substrate (SigmaFast™ BCIP®/NBT, Sigma-Aldrich, St. Louis, MO) or a 2% solution of Alizarin Red S [46] to show mineralization.

Immunohistochemical staining was also performed to monitor the differentiation progression of hMSCs into an osteogenic lineage using Endoglin (CD105) [47], a biomarker expressed in undifferentiated hMSCs and absent in mature osteoblasts, and osteocalcin [48] which is expressed only in mature osteoblasts. Briefly, hMSCs and cells treated with induction media for 21 days were seeded and grown overnight on gelatin-coated coverslips. Cells were directly labeled with FITC-conjugated anti-CD105 (1:200 dilution, Abcam). Osteocalcin was assessed by fixing cells and incubating with a primary anti-osteocalcin antibody (10 μg/mL, R&D Systems, Minneapolis, MN) for 3 hours at room temperature, and then incubating with a secondary antibody for 1 hour at room temperature (1:200 dilution, R&D Systems). Cells were counterstained with Hoechst 33342 to visualize the nuclei and imaged under an epi-fluorescent inverted microscope (NIKON Ti-U). In order to visualize hMSCs and osteoblasts and observe their migration trajectories in the DEP sorting device during operation, adherent cell populations were labeled with either CellTracker™ Green or CellTracker™ Red (Life Technologies) fluorescent dyes, according to manufacturer's instructions. Dyed hMSCs were dissociated with TrypLE Express dissociation reagent (Life Technologies) and osteoblasts were dissociated with 0.25% trypsin-EDTA and 1 mg/mL Type 2 collagenase (Worthington Biochemical, Lakewood, NJ). Equal numbers of MSCs and osteoblasts were mixed (0.7-1.0x10^6 cells/mL) and resuspended in a DEP buffer composed of 5.1% sucrose, 0.3% dextrose, and enough RPMI media to raise the conductivity to 200 μS/cm. In order to reduce cell adherence to surfaces, 0.2% bovine serum albumin was added to the buffer solution.

3.2 Device Fabrication

The microfluidic DEP sorter consists of two layers: a fluidic channel layer in PDMS, and an electrode layer on a glass substrate. SU8 soft lithography masters were developed for the PDMS layer. The

microfluidic channels were fabricated in PDMS by mixing the elastomer with a curing agent and curing it onto the SU8 channel masters. Gold electrodes were fabricated on Pyrex 7740 substrates using standard lithography techniques specifically developed for glass substrates [49]. Briefly, gold electrodes were fabricated by spin-coating a photoresist onto a clean glass wafer, exposing and developing the photoresist, depositing a 10 nm layer of chromium (for enhancing Au adhesion), followed by a 100 nm layer of gold using electron beam deposition, and then lifting off the photoresist layer, resulting in the desired electrode elements. For assembling the DEP sorter prototypes, the PDMS layer was bonded to the electrode wafer using plasma bonding. Figure 2 shows images of the fabricated microfluidic device. The width and length of the microfluidic channel was 2 mm and 13 mm, respectively, and the channel depth was 26 µm. The width of the sample inlet and buffer inlet was 250 µm and 1.75 mm, respectively. The interdigitated electrode array contained 50 electrodes, 50 µm in width with a gap of 50 µm.

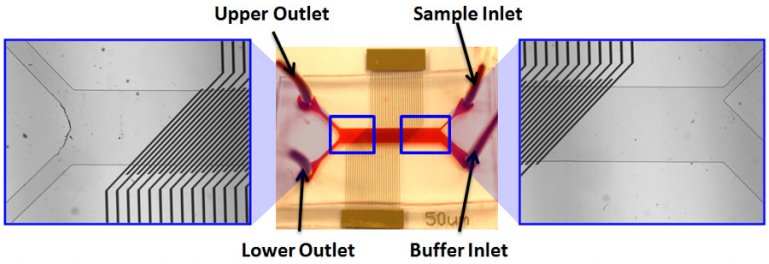

Figure 2. Fabricated DEP-based microfluidic device for stem cell separation. The magnified images on the left and right show the regions near the outlets and inlets, respectively. The middle image shows the assembled device including a PDMS channel bonded to lithographically patterned gold-on-glass electrodes with contact pads for electrical connections. The width and length of the microfluidic channel was 2 mm and 13 mm, respectively, and the channel depth was 26 µm. The interdigitated electrode array was made by depositing 100 nm gold on the glass substrate. A 10 nm layer of chromium was deposited between the gold layer and glass substrate to enhance the adhesion. The interdigitated electrode finger was 50 µm in width with a gap of 50 µm.

3.3 Experimental Setup

The experimental test protocol was established as follows: (1) prior to all experiments, the channel was coated with 0.5% BSA for 2 hours to reduce cell adhesion to the microchannel and electrode surfaces. The channel was washed using the DEP buffer for 5-10 minutes. (2) Cell samples containing a mix of hMSCs and osteoblasts, as described in Section 3.1, were injected into the device from the sample inlet. DEP buffer was injected into the buffer inlet through tubes connected to a syringe pump. Sample flow rates of 0.3 and 0.9 µl/min were investigated, along with corresponding buffer flow rates of 1.5 and 4.5 µl/min, respectively, maintaining a 5:1 sheath to sample flow ratio. (3) An AC frequency function generator, connected to the DEP device via the electrode pads, was used to apply an AC voltage between the electrodes. The AC field was alternated between on (with a duration of 0.7 s) and off (0.3 s). (4) Experimental results were observed using the Nikon Eclipse TE2000-U epi-fluorescence inverted microscope, and time-lapse images were recorded for analysis using a cooled CCD camera (Q-imaging Retiga EXi Fast 1394). Each experiment was performed from 10 minutes to 30 minutes depending on the flow rate to process at least a total volume of 50 µl. Samples of cells at both lower and upper outlets were collected and used for further quantitative analysis.

3.4 Quantitative Analysis

For corroboration, two independent methods were used to count the number (typically 100~300, depending on the flow rate of the sample solution) of hMSCs and osteoblasts exiting each outlet for quantitative evaluation of sorting performance. An on-chip cell count was performed by analyzing videos acquired during experiments using NIS Element software (Nikon Instruments Inc., Melville, NY). An off-chip hemocytometric analysis was used to count the number of hMSCs and osteoblasts collected at the two outlets and trypan blue assay was used to evaluate viability. Both collection efficiency and purity of hMSCs and osteoblasts at each outlet was calculated to characterize sorter performance. The collection efficiency was defined as the number of one cell type collected at one outlet divided by the

total number of this cell type collected at both outlets. The purity was defined as the number of the desired cell type at one outlet divided by the number of all cells collected at the same outlet.

4 Results and Discussion

The differentiation progression of hMSC-derived osteoblasts was evaluated by observing alkaline phosphatase activity and mineralization. Figure 3a and Figure 3b show an increase in alkaline phosphatase activity and mineralization over 21 days post-induction, indicating the presence of mature osteoblasts.

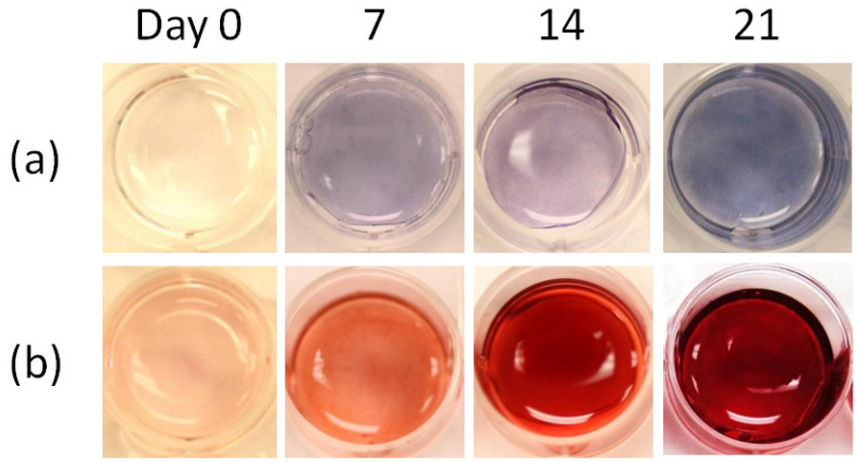

Figure 3. Progression of human mesenchymal stem cell differentiation was monitored by observing increases in (a) alkaline phosphatase activity, and (b) mineralization during the 21 day differentiation process.

Homogeneity of undifferentiated hMSCs and differentiated osteoblasts at 21 days post-induction populations was observed by immunocytochemical staining of CD105, an hMSC marker, and osteocalcin, a mature osteoblast marker. Figure 4 shows sample images of high purity of either hMSCs or osteoblasts in each cell population.

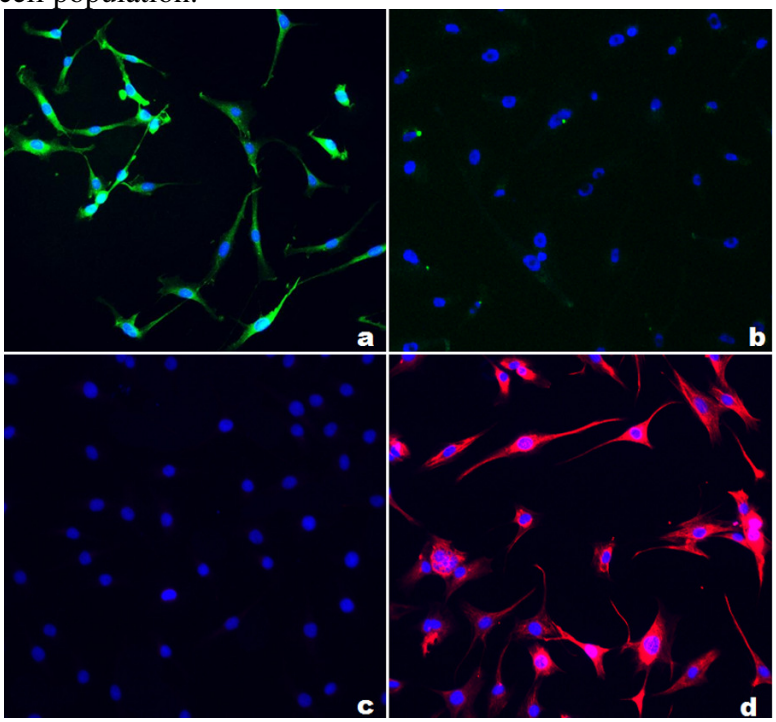

Figure 4. Human mesenchymal stem cells and cells differentiation into osteoblasts was evaluated using immunocytochemical staining of endoglin (CD105), present in undifferentiated cells (a) but significantly reduced in osteoblasts (b), and osteocalcin, not present in hMSCs (c), but appearing in mature osteoblasts (d).

Initial tests to separate the cells were carried out at a total flow rate of 1.8 µl/min (0.3 µl/min and 1.5 µl/min for the sample inlet and buffer inlet, respectively), along with an AC field of 7.2 V peak-to-peak at a frequency of 3 MHz (DEP spectra [50] of both hMSCs and osteoblasts were measured under various frequencies ranges from 10 kHz to 10 MHz and an optimized frequency of 3 MHz was obtained for the separation of hMSCs and osteoblasts). When the electric field was off, both hMSCs and osteoblasts flowed straight through the microchannel without any lateral displacement, and exited the channel via the upper outlet due to the hydrodynamic and sheath flow running in parallel (see Video_1 in electronic supplementary information (ESI)). When the electric field was applied using the alternating on-off strategy outlined previously, most of the osteoblasts (in green) experiencing stronger DEP forces were deflected laterally, followed zig-zig trajectories, and moved towards the lower outlet, whereas most of hMSCs (in red) remained on a straight trajectory due to weaker DEP force acting on them and exited via the upper outlet (see Video_2 in the ESI).

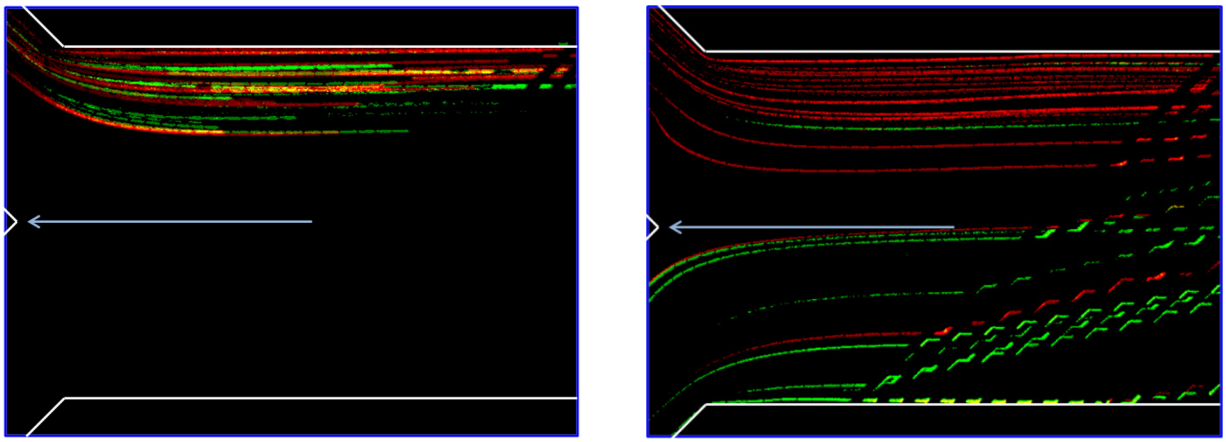

(a) (b)

Figure 5. The superimposed cell trajectories of hMSCs (in red) and osteoblasts (in green) under a flow rate of 1.8 µl/min (0.3 µl/min and 1.5 µl/min from the sample inlet and buffer inlet, respectively): (a) No electric field (field off); and (b) Alternating AC field of 7.2 V peak to peak at 3 MHz.

For better visualization, we superimposed the cell trajectories on the video into a single color image as shown in Figure 5. It is further verified that both hMSCs and osteoblasts moved in a straight path and exited via the upper outlet if there was no electric field (Figure 5a). When the AC field was on, most of osteoblasts were forced to the lower side of the channel and exited through the lower outlet, and the hMSCs continued to enter the upper outlet (Figure 5b). Although the ratio of hMSC (red) and osteoblast (green) was 1:1 for the inlet sample, most of the hMSCs were collected at the upper outlet and most of osteoblasts were collected at the lower outlet.

To quantitatively evaluate sorting performance, the collection efficiency and purity of hMSCs and osteoblasts at both outlets were calculated using the on-chip and off-chip analyses as described above, and are presented in Figure 6 and Figure 7. The results from the on-chip count indicate that 92% of hMSCs were collected in the upper outlet (8% escaped from the lower outlet), and 61% of differentiated osteoblasts were collected in the lower outlet (39% exited via the upper outlet). These results match the off-chip count, which shows 86% of hMSCs were collected in the upper outlet (14% escaped from the lower outlet) and 67% differentiated osteoblasts were collected in the lower outlet (33% from the upper outlet). Both hMSCs and osteoblasts showed greater than 95% viability using trypan blue assay. The purity of hMSCs at the upper outlet was 76% and 84% for on-chip and off-chip analysis, respectively, and the purity of the osteoblasts at the lower outlet was 85% and 65%. Compared to the initial sample with 50% purity for each cell type, the populations of the collected hMSCs at the upper outlet and osteoblasts at the lower outlet were enriched. It should be noted that several factors may contribute to the mixed DEP sorting behavior in both cell populations that adversely impact the collection efficiency and purity metrics: (1) non-uniformity of the size and dielectric property of hMSCs; and (2) heterogeneity in differentiation products, which may contain a small fraction of hMSCs or partially

differentiated (e.g., progenitor) cells, leading to the migration of some cells labeled in green towards the upper outlet (see Figure 5). This is confirmed by another experiment using a 50:50 mixing of cells and 15 µm beads that carry distinctly different dielectric properties. More than 90% collection efficiencies and purities could be achieved in our sorter device (data not shown).

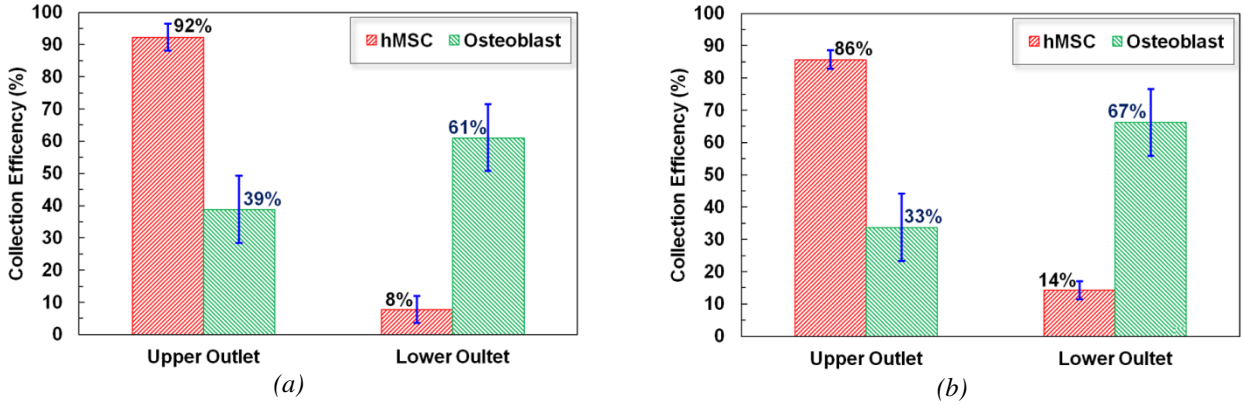

Figure 6. Collection efficiency of hMSCs and osteoblasts at different outlets, calculated from an (a) On-chip count; and an (b) Off-chip count. The flow rate was 1.8 µl/min (0.3 µl/min and 1.5 µl/min from the sample inlet and buffer inlet, respectively) and the AC voltage was 7.2 V peak to peak at 3 MHz.

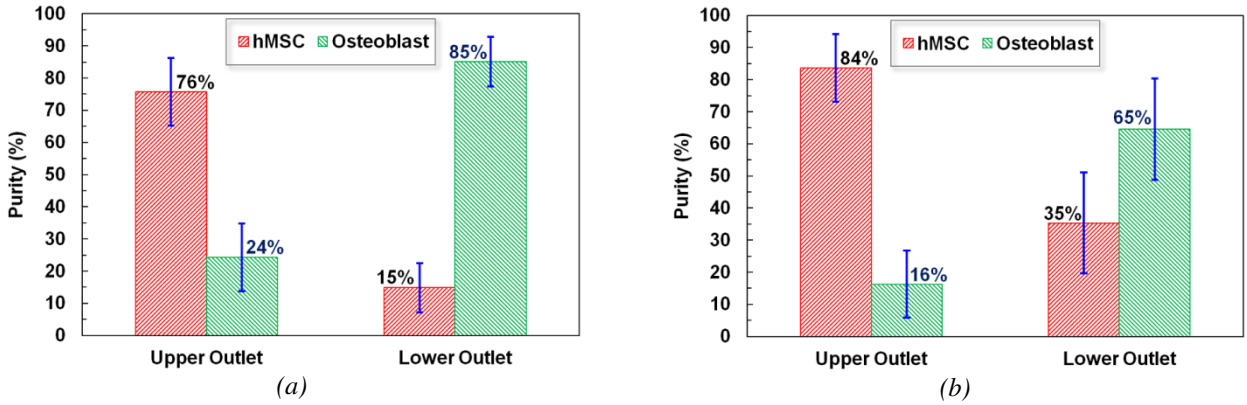

Figure 7. Purity of hMSCs and osteoblasts at different outlets, calculated from an (a) On-chip count; and an (b) Off-chip count. The flow rate was 1.8 µl/min (0.3 µl/min and 1.5 µl/min for the sample inlet and buffer inlet, respectively) and the AC voltage was 7.2 V peak to peak at 3 MHz.

Furthermore, we examined sorting performance of our device at a higher flow rate of 5.4 µl/min (0.9 µl/min and 4.5 µl/min from sample and buffer flow rate, respectively). The initial test used the same electric field as that for the low flow rate (i.e., 7.2 V peak to peak at 3 MHz). At this voltage, DEP force was not strong enough to deflect cells laterally due to increased hydrodynamic force under higher flow rate (see Video_3 in the ESI). Cell trajectories were graphically superimposed onto a single image as shown in Figure 8. All the hMSCs (in red) and most of osteoblasts (in green) exited through the upper outlet, and very few osteoblasts were directed to the lower outlet (Figure 8a). This indicated that the electric field was not sufficient. To generate stronger DEP force, we gradually increased the voltage and found more osteoblasts were deflected laterally. Successful separation was achieved when the voltage was raised to 15.4 V peak to peak at 3 MHz (high electric field, see Video_4 in the ESI). Most of osteoblasts were deflected, and exited through the lower outlet, while most of hMSCs stayed on the straight trajectory and exited through the upper outlet (Figure 8b), leading to effective separation of hMSCs and osteoblasts.

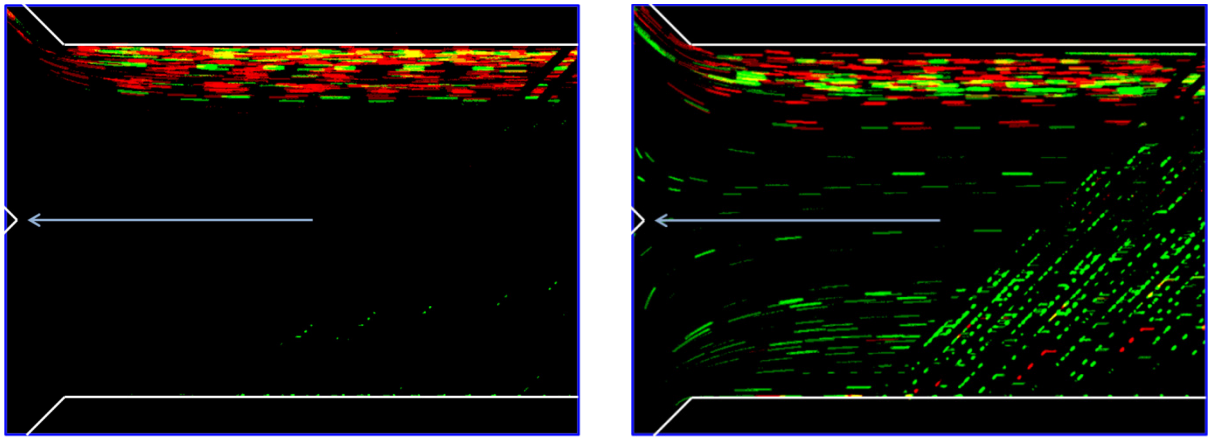

(a) (b)

Figure 8. Superimposed cell trajectories of hMSCs (in red) and osteoblasts (in green) under a higher flow rate 5.4 µl/min (0.9 µl/min and 4.5 µl/min for the sample inlet and buffer inlet, respectively): (a) Alternating AC field of 7.2 V peak to peak at 3 MHz; (b) Alternating AC field of 15.4 V peak to peak at 3 MHz.

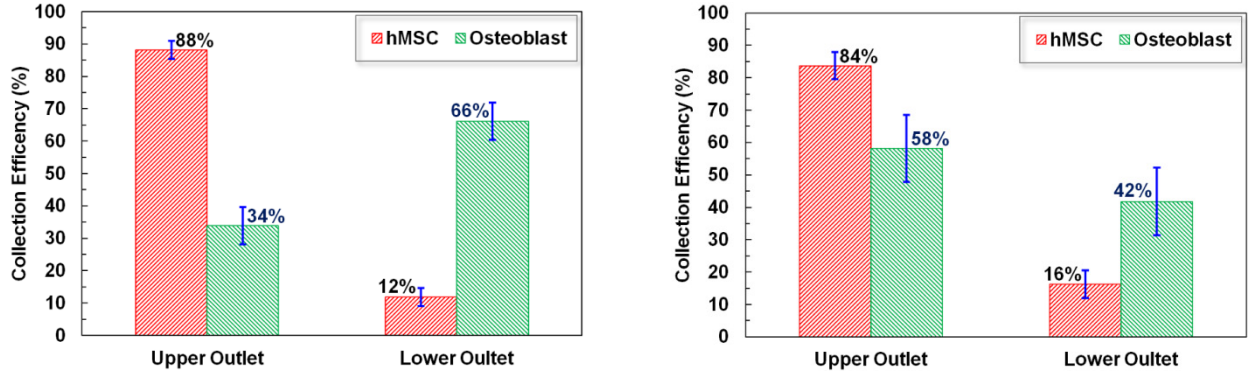

(a) (b)

Figure 9. Collection efficiency of hMSCs and osteoblasts at different outlets, calculated from (a) On-chip count; and (b) Off-chip count. The flow rate was 5.4 µl/min (0.9 µl/min and 4.5 µl/min for the sample inlet and buffer inlet, respectively) and the AC voltage was 15.4 V peak to peak at 3 MHz.

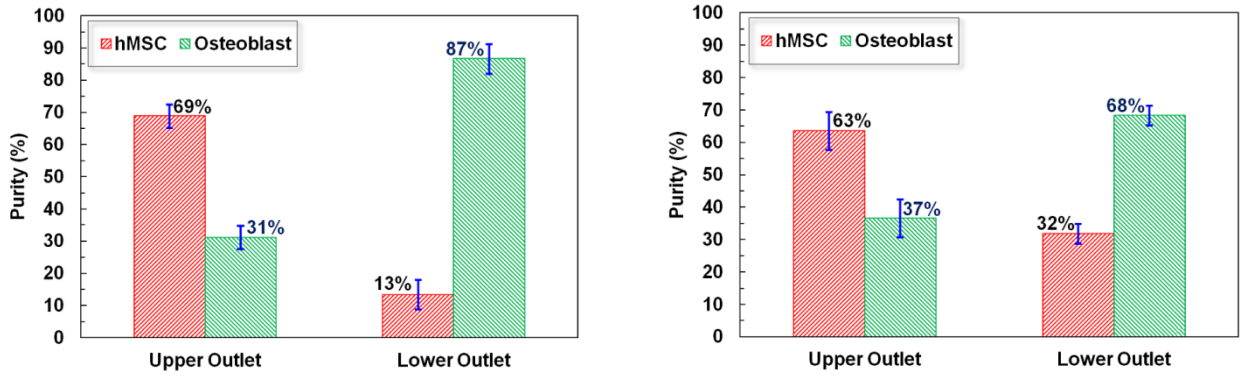

(a) (b)

Figure 10. Purity of hMSCs and osteoblasts at different outlets, calculated from (a) On-chip count; and (b) Off-chip count. The flow rate was 5.4 µl/min (0.9 µl/min and 4.5 µl/min for the sample inlet and buffer inlet, respectively) and the AC voltage was 15.4 V peak to peak at 3 MHz.

The collection efficiency and purity of hMSCs and osteoblasts at different outlets for the higher flow rate were also calculated using the on-chip and off-chip analysis as described above, which are shown in Figure 9 and Figure 10, respectively. The collection efficiency for hMSCs at the upper outlet was 88% and 84% based on the on- and off-chip analysis, and hMSC purity was 69% and 63%. The collection efficiency for osteoblasts at the lower outlet was 66% and 42% according to the on- and off-chip analysis, and the purity of osteoblasts was 87% and 68%. The purity of each cell population collected

from the device markedly improved from 50% –the initial value at the inlet—confirming the effectiveness of the DEP-based separation of the hMSCs and osteoblasts.

5 Conclusions

In this paper, we presented a continuous-flow, microfluidic DEP device to separate stem cells and their differentiation products. The device combines the accumulation of dielectrophoresis (DEP) force realized in a large array of oblique interdigitated electrodes and the alternating field control to enable continuous sorting operation, and hence, saliently enhances the cell recovery and collection efficiency. Extensive experimental testing was carried out to demonstrate the functionality of the device and to characterize its performance. Important technical findings are summarized as follows:

(1) It was found that the optimal frequency generating the salient difference in Re(β) between hMSCs and their differentiation progenies (i.e., osteoblast in this study) falls into the positive DEP regime, where many cells can be slowed down or even trapped at the electrode edges. DEP sorting that allows cells to traverse the electrodes in concert with alternating AC field was shown to be effective to address the issue and allow continuous operation.

(2) Experiments demonstrated notable separation of hMSCs and osteoblasts. Most of osteoblasts experiencing stronger DEP forces were deflected laterally and continuously, following zig-zig trajectories, and moved towards the lower outlet, whereas most of hMSCs remained on a straight trajectory and exited via the upper outlet due to weaker DEP force.

(3) The collection efficiency and purity for hMSCs and osteoblasts were measured, exhibiting consistent performance even when the flow rate/throughput was increased three-fold (from 1.8 to 5.4 µl/min). Collection efficiency up to 92% can be obtained for hMSCs at the upper outlet, with a purity up to 84%, and the collection efficiency approaches up to 67%, and the purity up to 87%, for osteoblasts in the other outlet. The heterogeneous DEP sorting behavior in both cell populations can potentially be attributed to the non-uniformity in cell sizes and dielectric property as well as the partial differentiation of hMSCs.

Our studies firmly establish the feasibility of the microfluidic DEP sorter for continuous, label-free sorting of hMSC and its differentiation products. Future developments will focus on improving the processing throughput and applying the technique to other stem cell categories (e.g., iPSC) and various differentiation lineages.

Acknowledgment

This research was sponsored by the U.S. Army Medical Research and Materiel Command (USAMRMC) under SBIR contract No. W81XWH-12-C-0069. GJK and LMA acknowledge Dr. Alan Perantoni and Ms. Nirmala Sharma of the Cancer and Developmental Biology Laboratory providing access to specialized tissue culture facilities and for discussions regarding analysis of differentiation and development markers.

Reference:

1. DiMarino, A.M., A.I. Caplan, and T.L. Bonfield, *Mesenchymal stem cells in tissue repair.* Frontiers in immunology, 2013. **4**.
2. Harting, M.T., et al., *Intravenous mesenchymal stem cell therapy for traumatic brain injury: Laboratory investigation.* Journal of neurosurgery, 2009. **110**(6): p. 1189.
3. Hentze, H., R. Graichen, and A. Colman, *Cell therapy and the safety of embryonic stem cell-derived grafts.* Trends in biotechnology, 2007. **25**(1): p. 24-32.
4. Hwang, N.S., et al., *Mesenchymal stem cell differentiation and roles in regenerative medicine.* Wiley Interdisciplinary Reviews: Systems Biology and Medicine, 2009. **1**(1): p. 97-106.

5. Castagnola, A., S. Eda, and J. Jurat-Fuentes, *Monitoring stem cell proliferation and differentiation in primary midgut cell cultures from< i> Heliothis virescens</i> larvae using flow cytometry.* Differentiation, 2011. **81**(3): p. 192-198.
6. Uchida, N., et al., *Direct isolation of human central nervous system stem cells.* Proceedings of the National Academy of Sciences, 2000. **97**(26): p. 14720-14725.
7. Nardi, N.B. and L. da Silva Meirelles, *Mesenchymal stem cells: isolation, in vitro expansion and characterization*, in *Stem Cells*. 2006, Springer. p. 249-282.
8. Angstmann, M., et al., *Monitoring human mesenchymal stromal cell differentiation by electrochemical impedance sensing.* Cytotherapy, 2011. **13**(9): p. 1074-1089.
9. Bagnaninchi, P.O. and N. Drummond, *Real-time label-free monitoring of adipose-derived stem cell differentiation with electric cell-substrate impedance sensing.* Proceedings of the National Academy of Sciences, 2011. **108**(16): p. 6462-6467.
10. Bieberich, E. and A. Guiseppi-Elie, *Neuronal differentiation and synapse formation of PC12 and embryonic stem cells on interdigitated microelectrode arrays:: Contact structures for neuron-to-electrode signal transmission (NEST).* Biosensors and Bioelectronics, 2004. **19**(8): p. 923-931.
11. Hildebrandt, C., et al., *Detection of the osteogenic differentiation of mesenchymal stem cells in 2D and 3D cultures by electrochemical impedance spectroscopy.* Journal of biotechnology, 2010. **148**(1): p. 83-90.
12. Park, H.E., et al., *Real-time monitoring of neural differentiation of human mesenchymal stem cells by electric cell-substrate impedance sensing.* BioMed Research International, 2011. **2011**.
13. Song, H., et al., *A microfluidic impedance flow cytometer for identification of differentiation state of stem cells.* Lab on a Chip, 2013. **13**(12): p. 2300-2310.
14. Pethig, R., *Review article—dielectrophoresis: status of the theory, technology, and applications.* Biomicrofluidics, 2010. **4**(2): p. 022811.
15. Becker, F., et al., *The removal of human leukaemia cells from blood using interdigitated microelectrodes.* Journal of Physics D: Applied Physics, 1994. **27**(12): p. 2659.
16. Chen, D., H. Du, and W. Li, *Bioparticle separation and manipulation using dielectrophoresis.* Sensors and Actuators A: Physical, 2007. **133**(2): p. 329-334.
17. Gascoyne, P.R., et al., *Dielectrophoretic separation of cancer cells from blood.* Industry Applications, IEEE Transactions on, 1997. **33**(3): p. 670-678.
18. Gupta, V., et al., *ApoStream™, a new dielectrophoretic device for antibody independent isolation and recovery of viable cancer cells from blood.* Biomicrofluidics, 2012. **6**(2): p. 024133.
19. Han, K.-H., S.-I. Han, and A.B. Frazier, *Lateral displacement as a function of particle size using a piecewise curved planar interdigitated electrode array.* Lab on a Chip, 2009. **9**(20): p. 2958-2964.
20. Hu, X., et al., *Marker-specific sorting of rare cells using dielectrophoresis.* Proceedings of the National Academy of Sciences of the United States of America, 2005. **102**(44): p. 15757-15761.
21. Huang, Y., et al., *The removal of human breast cancer cells from hematopoietic CD34+ stem cells by dielectrophoretic field-flow-fractionation.* Journal of hematotherapy & stem cell research, 1999. **8**(5): p. 481-490.
22. Kim, U., et al., *Multitarget dielectrophoresis activated cell sorter.* Analytical chemistry, 2008. **80**(22): p. 8656-8661.
23. Li, M., et al., *Improved concentration and separation of particles in a 3D dielectrophoretic chip integrating focusing, aligning and trapping.* Microfluidics and nanofluidics, 2013. **14**(3-4): p. 527-539.
24. Li, S., et al., *High-throughput particle manipulation by hydrodynamic, electrokinetic, and dielectrophoretic effects in an integrated microfluidic chip.* Biomicrofluidics, 2013. **7**(2): p. 024106.

25. Ling, S.H., Y.C. Lam, and K.S. Chian, *Continuous cell separation using dielectrophoresis through asymmetric and periodic microelectrode array.* Analytical chemistry, 2012. **84**(15): p. 6463-6470.
26. Park, J., et al., *An efficient cell separation system using 3D-asymmetric microelectrodes.* Lab on a Chip, 2005. **5**(11): p. 1264-1270.
27. Prasad, S., et al., *Separation of individual neurons using dielectrophoretic alternative current fields.* Journal of neuroscience methods, 2004. **135**(1): p. 79-88.
28. Sano, M.B., et al., *Contactless dielectrophoretic spectroscopy: examination of the dielectric properties of cells found in blood.* Electrophoresis, 2011. **32**(22): p. 3164-3171.
29. Shim, S., et al., *Antibody-independent isolation of circulating tumor cells by continuous-flow dielectrophoresis.* Biomicrofluidics, 2013. **7**(1): p. 011807.
30. Song, H., et al., *Continuous-mode dielectrophoretic gating for highly efficient separation of analytes in surface micromachined microfluidic devices.* Journal of Micromechanics and Microengineering, 2008. **18**(12): p. 125013.
31. Wang, X.-B., et al., *Cell separation by dielectrophoretic field-flow-fractionation.* Analytical Chemistry, 2000. **72**(4): p. 832-839.
32. Pethig, R., et al., *Dielectrophoresis: a review of applications for stem cell research.* BioMed Research International, 2010. **2010**.
33. Flanagan, L.A., et al., *Unique dielectric properties distinguish stem cells and their differentiated progeny.* Stem Cells, 2008. **26**(3): p. 656-665.
34. Labeed, F.H., et al., *Biophysical characteristics reveal neural stem cell differentiation potential.* PloS one, 2011. **6**(9): p. e25458.
35. Nourse, J., et al., *Membrane biophysics define neuron and astrocyte progenitors in the neural lineage.* STEM CELLS, 2013.
36. Prieto, J.L., et al., *Frequency discretization in dielectrophoretic assisted cell sorting arrays to isolate neural cells.* Lab on a Chip, 2012. **12**(12): p. 2182-2189.
37. Stephens, M., et al., *The dielectrophoresis enrichment of CD34+ cells from peripheral blood stem cell harvests.* Bone marrow transplantation, 1996. **18**(4): p. 777-782.
38. Talary, M., et al., *Dielectrophoretic separation and enrichment of CD34+ cell subpopulation from bone marrow and peripheral blood stem cells.* Medical and Biological Engineering and Computing, 1995. **33**(2): p. 235-237.
39. Vykoukal, J., et al., *Enrichment of putative stem cells from adipose tissue using dielectrophoretic field-flow fractionation.* Lab on a Chip, 2008. **8**(8): p. 1386-1393.
40. Jones, T.B. and T.B. Jones, *Electromechanics of particles*. 2005: Cambridge University Press.
41. Holmes, D., et al. *On-chip high-speed sorting of micron-sized particles for high-throughput analysis*. in *IEE Proceedings-Nanobiotechnology*. 2005. IET.
42. Okamoto, T., et al., *Clonal heterogeneity in differentiation potential of immortalized human mesenchymal stem cells.* Biochemical and biophysical research communications, 2002. **295**(2): p. 354-361.
43. Rodrigues, M., et al., *Surface Tethered Epidermal Growth Factor Protects Proliferating and Differentiating Multipotential Stromal Cells from FasL‐Induced Apoptosis.* Stem Cells, 2013. **31**(1): p. 104-116.
44. Bourgine, P.E., et al., *Tissue decellularization by activation of programmed cell death.* Biomaterials, 2013. **34**(26): p. 6099-6108.
45. Nicolaidou, V., et al., *Monocytes induce STAT3 activation in human mesenchymal stem cells to promote osteoblast formation.* PloS one, 2012. **7**(7): p. e39871.
46. Sila-Asna, M., et al., *Osteoblast differentiation and bone formation gene expression in strontium-inducing bone marrow mesenchymal stem cell.* Kobe J Med Sci, 2007. **53**(1-2): p. 25-35.

47. Schieker, M., et al., *Human mesenchymal stem cells at the single‐cell level: simultaneous seven‐colour immunofluorescence.* Journal of anatomy, 2007. **210**(5): p. 592-599.
48. Kulterer, B., et al., *Gene expression profiling of human mesenchymal stem cells derived from bone marrow during expansion and osteoblast differentiation.* BMC genomics, 2007. **8**(1): p. 70.
49. Song, H., et al., *Chaotic mixing in microchannels via low frequency switching transverse electroosmotic flow generated on integrated microelectrodes.* Lab on a Chip. **10**(6): p. 734-740.
50. Kaler, K. and T. Jones, *Dielectrophoretic spectra of single cells determined by feedback-controlled levitation.* Biophysical journal, 1990. **57**(2): p. 173-182.